Experimental Analysis of Resistance to Electrocorosion of a High Chromium Cast Iron with Applications in the Vehicle Industry

COSTEL DOREL FLOREA[1], IOAN CARCEA[1], RAMONA CIMPOESU[1], STEFAN LUCIAN TOMA[1], IOAN GABRIEL SANDU[1,2], COSTICA BEJINARIU[1]*

[1] Gheorghe Asachi Technical University of Iasi, Faculty of Materials Science and Engineering, 67 D. Mangeron Blvd., 700050, Iasi, Romania

[2] Romanian Inventors Forum, 3 Sf. Petru Movila Str., 700089, Iasi, Romania

We obtained a new Fe-C material, a cast iron with high chromium content. The experimental material was analyzed by microstructural (SEM electronic) and chemical (EDAX characteristic X-ray dispersive energy analysis) point of view. The addition of chromium is aimed to increase the corrosion resistance and durability of FC250 castings used on industrial scale in the manufacture of automotive brake discs. The material was obtained using an industrial scale furnace. The experimental results showed a substantial increase in corrosion resistance by the addition of chromium.

Keywords: high Cr cast iron, industrial furnace, SEM, EDS

Due to the continuous increase in vehicle component demands, it is necessary to use new materials with special properties to cover the full range of requirements of automotive systems in operation. The same applies to braking systems where the running requirements are in continuous growth, and common materials such as FC250 cast iron brake discs, no longer meet the standard characteristics, reducing the safety and efficiency of the vehicle.

The usual material used for the brake system in the automotive industry is cast iron. The specific mass and weight of the cast iron is higher, which leads to higher fuel consumption. Cast iron with carbon content (C) of 2-4% dissolved in the matrix is known as gray iron due to the specific color [1, 2]. In view of the low cost, the ease with which it is obtained and the thermal stability, this cast iron (gray cast iron) is the main choice for the material for the brake discs. For a good performance of the discs, they must be produced in a foundry where the chemical composition and the cooling process are closely monitored to control the shape, distribution and type of graphite. This is necessary to minimize deformations during mechanical machining to provide good wear, vibration, and crack resistance [3-7].

Chromium, in quantitative terms, varies in the casting of the oligo-element (less than 0.3%wt) to the alloying element of more than 0.3%wt. Chromium is an antigraffitizer on a scale, in increasing order of the anti-grafitizing (whitening) effect, the order being: W, Mn, Mo, Sn, Cr, V, B etc. As an antigraffitizer, chromium increases the number of eutectic cells and the proportion of perlite, in the case of gray cast iron [8]. At eutectoid temperature (in the Fe-C binary system) or in the eutectoid temperature range (in the case of industrial cast iron), chromium prevents diffusion processes and reduces the austenite transformation temperature. Chromium is an alfagen element - it favors the development of the occupied field of gamma ferrite in the equilibrium diagrams. The perlite effect of chromium from eutectic transformation results from the comparison with other chemical elements by means of relative coefficients of influence having the following values: Cu 1.0%, Ni 0.2%, Mn 0.5%, V 1.0%, Sn 1.2%, Mo and Cr ≤ 1.0%. In principle, chromium has different significant influences as cast iron is low, medium or highly alloyed [9].

The chromium content is depending on the purpose of the cast iron, being 11 ... 30% for the wear-resistant cast iron, 15 ... 25% and 29 ... 35% for the high temperature cast iron and 20 ... 35% for the cast iron corrosion. In this article a cast iron with 21 wt% Cr was chosen to combine wear and corrosion resistance characteristics [10].

The core of a cylindrical or conical colony - crystallization germs - is the elongated carbide $(Fe,Cr)_7C_3$. The austenitic cylindrical colonies (austenite wraps the carbine branches) and the carbide $(Fe,Cr)_7C_3$ grow in the form of beams, forming cementations eutectic Fe_3C eutectic and cellular eutectic austenite. If the chromium proportion is greater than 13%, the cementite disappears from the structure, i.e. the eutectic colonies disappear in the form of parallelepiped blocks (cellular structure), the eutectic being formed only from austenite cylindrical colonies and carbide $(Fe,Cr)_7C_3$ [11]. For these castings, there is the liquid faze and austenitic faze, in the equilibrium diagram, for hypoeutectic cast iron in the range between the liquidus and solidus curves, and for the hypereutectic cast iron in the range between the liquidus and solidus curves there is liquid and carbide $(Fe,Cr)_7C_3$, (the primary carbide is hexagonal) [12].

The metallographic structure of high-alloy cast iron is made up of eutectic carbides in a chromium-alloyed ferrite mass (for cast iron with a chromium content of less than 13%, in the structure there are also phase - perlite of ferrite and carbide $(Fe,Cr)_3C$). The metallic load is made up of high-purity steel waste, own waste, ferro-chromium and ferro-molybdenum or molybdenum oxide [13].

Chromium alloying stage is only made in the furnace. Chromium losses during manufacture are up to 5%. Characteristic of chromium-alloyed cast iron is the alloying with nitrogen, alloying by the use of nitrogen-containing ferro-chromium - introduction of sodium ferrocyanide into the metal bath of the furnace - introduction of urea, sodium nitrate, potassium nitrate into the casting pot, calcium cyanamide, hexamethylenetetramine, ammonia, ammonium chloride and sodium nitrite, etc. It is preferred to use in practice compositions as close as possible to the eutectic ones due to high liquid shrinkage which would

* email: costica.bejinariu@yahoo.com

require the use of large carpets (the solidification shrinkage is close to that of the steels) [14].

In this paper are presented the experimental results obtained from the microstructural and chemical characterization of a new metallic material (cast iron with a high percentage of chromium) as compared to one with industrial applications (FC250).

Experimental part

Experimental samples with different chromium percentages were obtained as thermally treated ingots and from which experimental samples were dispensed. For the present study, in addition to a classic FC 250 cast iron, three types of chromium alloy cast iron were developed at SC RANCON SRL Ia°i in the induction furnace and cast into molds made of KALHARTZ 8500 resin casting compound and hardener HARTER. In cast irons with 20…30%wt Cr is recommended the inoculation with 0.05 ... 0.1% Al, where sulphides are spheroidised (improve most of the characteristics) or 0.2% ferrocerium (the sulfur content is reduced by 20%, the structure finishes and non-metallic inclusions are spheroidized). It is recommended that the casting temperature be at least 1400°C because of the compact oxide film present on the surface of the liquid casting which causes the film to form on the surface of the molded parts, but it should in principle be as small as possible. High-chromium alloys can be cast in rough, dry and permanent forms [15-17].

Two metallic samples were analyzed by the corrosion resistance point of view. The standard FC 250 cast iron and the new high chromium cast iron were mechanically polished till 2000 grid, experimental electrodes were made for electro-corrosion resistance experiments. A potentiostat equipment with a three electrodes cell was used for tests in a saline electrolyte solution. After the electrochemical experiments (linear and cyclic potentiometry) the material was cleaned by sonication for 60 min in technical alcohol [18]. The experimental samples surface was analyzed using SEM equipment (scanning electron microscopy with VegaTescan LMH II, VegaT software for 2 and 3D characterization) and EDAX detector (X-ray energy dispersive spectroscopy, Bruker type, Esprit software) for structural and chemical analyses [19-26].

Results and discussions

For corrosion resistance analysis of standard cast iron (FC250: C 3.1%, Si 1.2%, Mn 1.0%, P 0.03%, S 0.04%, C 2.64%, Si 1.11%, Mn 0.66%, P 0.03%, S 0.04%, Cr 0.21, Mo 0.1%) a potentiostat was used. Tests were performed on mechanically prepared samples by grinding in a standard saline solution (0.9% NaCl). The results are more qualitative and only partially quantitative in compliance with the G102-89 standard of testing in 2010: Standard practice for calculating corrosion speed and information obtained from electrochemical measurements.

Figure 1 shows the results obtained during the corrosion test, respectively the Tafel linear diagram and the cyclical diagram corresponding to the two analyzed materials: FC250, initial and cast iron C.

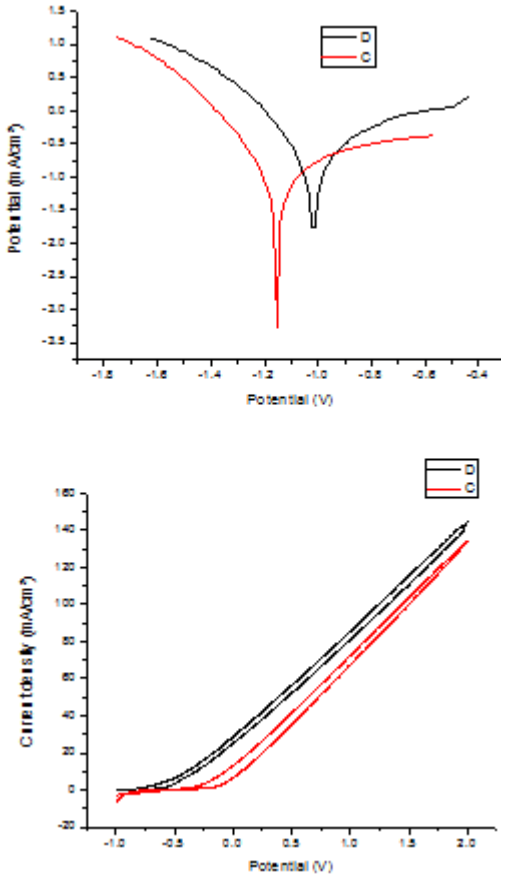

Fig.1. The behavior of the two experimental alloys D (FC250) and C (high alloyed with chromium) in saline solution: a. The Tafel linear diagram; b. Cyclical diagram

From the cyclic diagrams, it is observed that both materials exhibit a generalized corrosion on the entire surface of the material and without large dimensional variations over the analyzed range. The quantitative results recorded on the potentiostat equipment are shown in table 1. Even if the potential voltage 0, E_0 is close to the two samples, a large difference in polarization resistance is observed which leads to an increase in the corrosion rate of 2.26 times great for FC250 cast iron.

High chromium cast iron C has a lower corrosion rate than the initial sample, as can be seen from the Tafel diagrams corresponding to the two samples - figure 1a, and this increase in corrosion resistance is due both to chromium compounds and passivation of the iron matrix in this solution.

Surface analysis of corroded materials was done by electronic microscopy and EDAX chemical analysis. Figure 2 shows the surfaces of the two FC250 with 21 wt% Cr (fig. 2a, b, c and d). In both cases there is a homogeneous corrosion of the metal surface and formation of compounds on the surface of the material following the corrosion process. In both cases, the structure of the material is highlighted by selective corrosion, especially in cast iron C, of one of the phases. In the case of FC250, a strong corrosion is observed throughout the exposed area.

Table 1

PARAMETERS OF CORROSION RESISTANCE ANALYSIS PARAMETERS DURING LINEAR AND CYCLIC POTENTIOMETRY

Sample	E_0 mV	b_a mV	b_c mV	R_p ohm·cm²	J_{cor} mA/cm²	V_{cor} mm/year
D cast iron	-1017.0	660.4	-348.3	323.57	0.1377	3.645
C cast iron	-1150.2	874.8	-279.3	694.57	0.1312	1.610

In case of cast iron C, figure 2c and d, a particular corrosion of chromium dendrites is observed, noting that the basic iron-based matrix of Cr-dendrites was very poorly affected. It can be seen on the surface of the sample, especially that of dendrites, the formation of metal compounds, figure 2d, of micron or submicron size, which are stable on the surface of the metallic material. New compounds are preferably formed from the interface between chromium carbides and iron matrix, figure 2d.

In the table in figure 3, qualitative data are given, the energy spectrum characteristic of the chemical elements identified, and quantitatively the elements observed on the surface of the initial FC250 cast iron after the corrosion test. The quantitative data are presented both in percentage by weight (wt%) and in atomic percent (at%) and the EDAX element identification error in this case is mentioned. From the quantitative data analysis, the table in figure 3, there is a considerable iron loss on the surface of the sample which resulted in the percentage increase of the other elements in the material: C, Si and Mn forming more stable and corrosion-resistant compounds.

In general, a significant influence on the cast iron corrosion is due to the presence of chlorine ions, and the deficiency of chlorine on the corroded surface involves the removal of metallic compounds with chlorine in the electrolyte solution. Figure 4 shows the distribution of the chemical elements identified on the surface of the cast

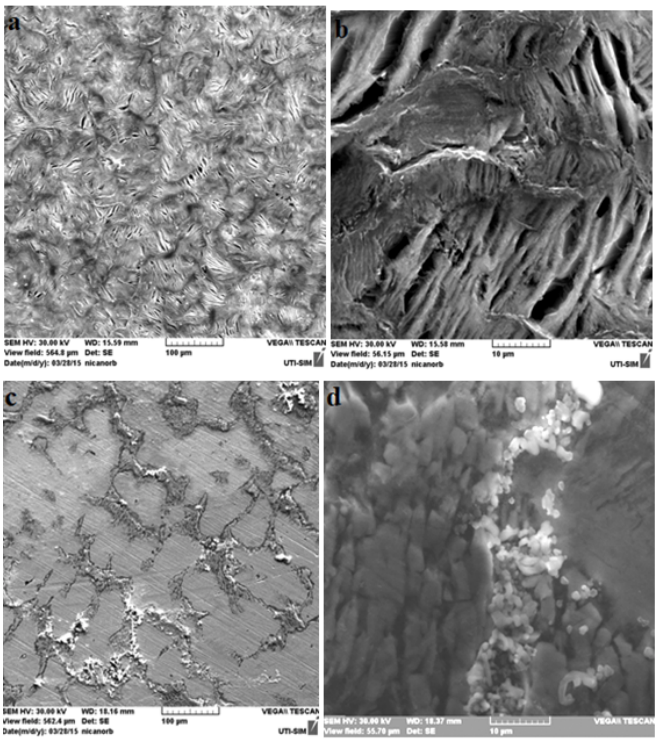

Fig. 2. SEM micrographs on the surface of corroded materials: a. and b. For standard cast iron FC 250; c. and d. for cast iron with high Cr content (Cr = 21% by weight)

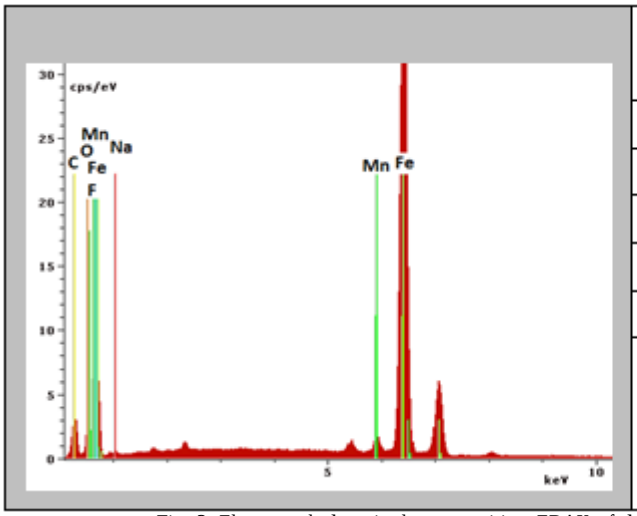

Chemical Elements	wt%	at %	Error %
Fe	75.35	47.31	1.86
O	9.48	20.79	1.56
C	7.05	20.57	1.06
Na	3.91	5.96	0.34
Si	2.21	4.08	3.66
Mn	2.00	1.28	0.11

Fig. 3. Elemental chemical composition EDAX of the sample surface D (9 mm^2) after the corrosion test

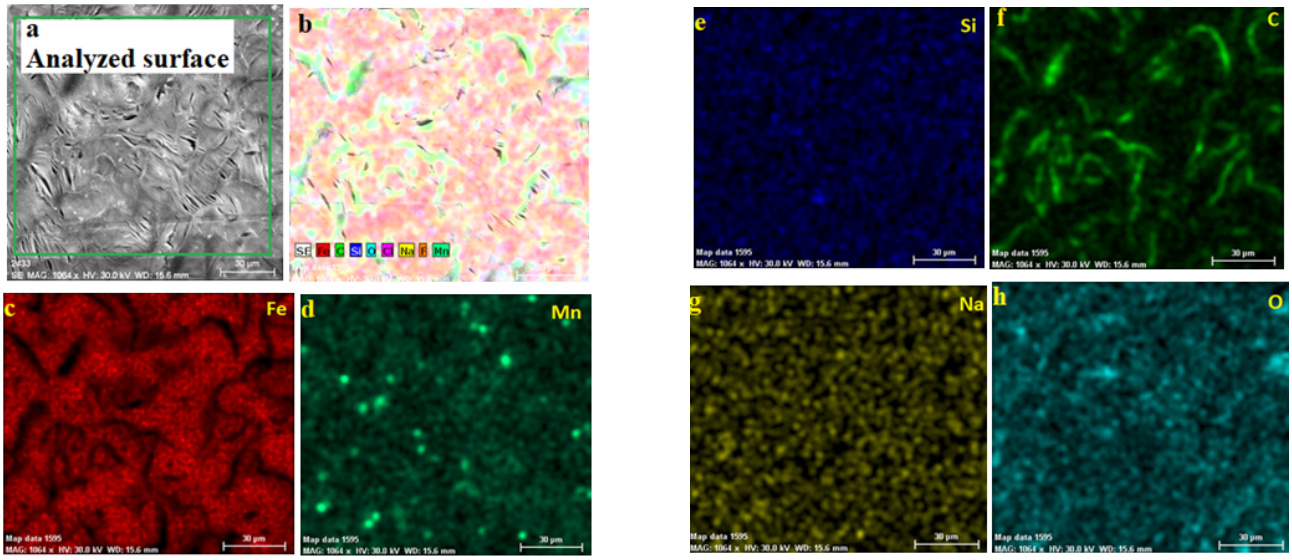

Fig. 4. Distribution of the identified chemical elements on the cast iron surface FC250 after corrosion: a. selected area for distribution; b. distribution of all elements; c. Fe; d. Mn; e. Si; f. C; g. Na and h. O

iron FC250 after corrosion, in a representative area (fig. 4a) containing all the elements identified (fig. 4b) and sequentially represented on Fe elements (fig. 4c) , Mn (fig 4d), Si (fig 4e), C (fig 4f), Na (fig 4g) and O (fig 4h).

The vermicular graphite formations as well as the manganese compounds are evidenced by the corrosion attack. It is noted, on the right side of the distribution in figure 4b and in the distribution of figure 4h occurrence of oxides on the material surface confirmed and by the high percentage of oxygen identified and shown in the table in figure 3.

Figure 5a shows the energy spectrum characteristic of the elements identified on the corroded surface of cast iron C (high alloyed with chromium). The presence of iron (Fe, Cr, C and Si) elements as well as some elements that have passed from the electrolyte solution to the metallic surface and formed various compounds (Na, O, Cl) are observed on the surface. In figure 5b shows three areas (1-3) selected for analyzing the chemical composition in dot (90 nm spot) on the surface of the metallic material. The three areas were selected as follows: 1 point analysis on the iron matrix, point 2 on dendrite (Cr,Fe)C and point 3 on a compound formed by the electro-corrosion test.

Table 2 shows the chemical compositions obtained on the total surface of figure 4b and points 1-3 on micrographs. Figure 4b highlights the selective attack that occurred in

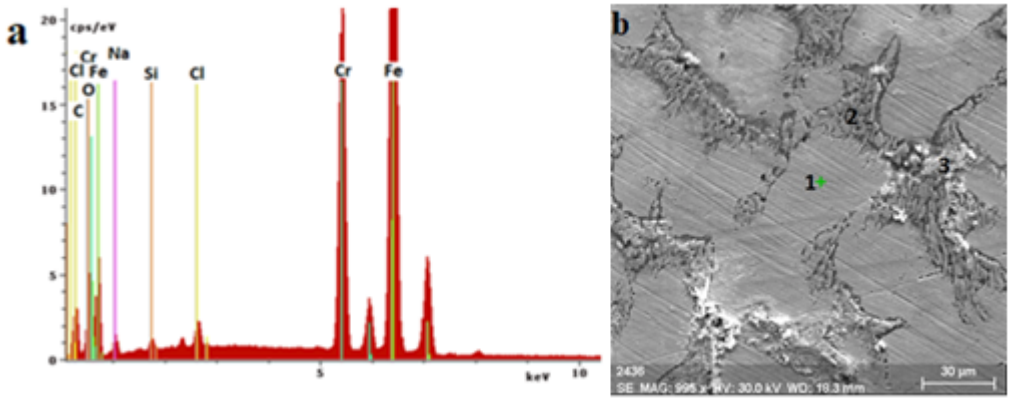

Fig. 5. Chemical surface area of the experimental sample C after corrosion:
a. Spectrum of energy specific to the chemical elements identified on the surface;
b. the chemical analysis area and the selection of three analysis points

Table 2

THE CHEMICAL COMPOSITION OF A 0.0144 mm² SURFACE AND THREE POINTS SELECTED IN FIGURE 5b ON A 90 nm SPOT, ALL RESULTS CARRIED OUT IN AUTOMATIC ANALYSIS

	Fe		Cr		Na		O		C		Cl		Si	
	wt %	at%	wt %	at%	wt %	at%	wt %	at%	wt %	at%	wt %	at%	wt %	at%
Area (0.0144 mm²)	61.51	45.89	22.01	17.6	6.6	11.9	5.9	15.4	1.8	6.3	1.2	1.47	0.9	1.3
Point 1 (0.25434 µm²)	78.14	68.6	17.7	16.7	-	-	-	-	3.2	12.9	-	-	1.04	1.8
Point 2 (0.25434 µm²)	33.3	25.9	56.4	47.3	-	-	3.72	10.14	3.47	12.6	3.19	3.92	-	-
Point 3 (0.25434 µm²)	32.9	22.9	50.37	37.8	-	-	9.9	24.2	3.5	11.4	3.3	3.6	-	-
EDAX Error	1.5		0.8		1.2		1.3		0.5		0.1		0.1	

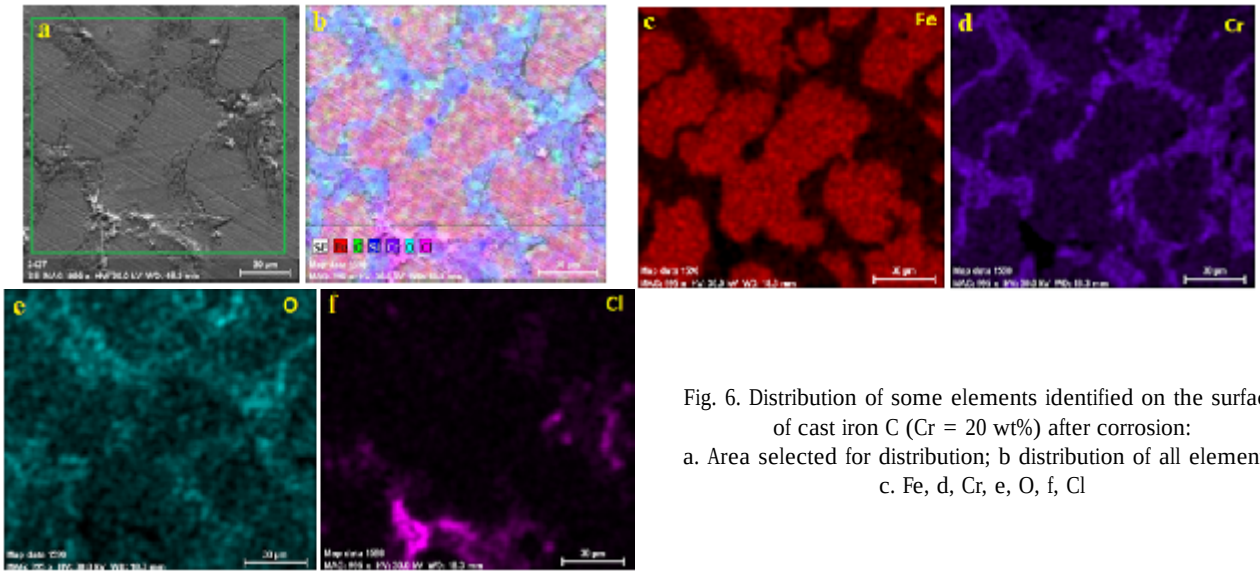

Fig. 6. Distribution of some elements identified on the surface of cast iron C (Cr = 20 wt%) after corrosion:
a. Area selected for distribution; b distribution of all elements; c. Fe, d, Cr, e, O, f, Cl

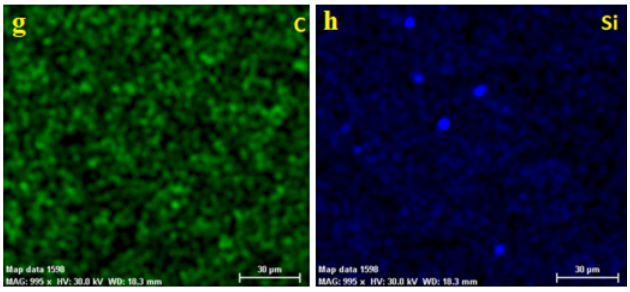

Fig. 6. Distribution of some elements identified on the surface of cast iron C (Cr = 20 wt%) after corrosion: g. C, and h. Si

the saline solution, the surface of the iron-based matrix, point 1, being intact from a microstructural point of view. At the same time, the Cr-based dendrites were observed during the electro-corrosion test. The chemical composition obtained from the general surface area of the sample, respectively, of the area in table 2, is close to the chemical composition obtained on the spark spectrometer and shows traces of new O, Na or Cl compounds.

Table 2 shows that there is no trace of oxidation or compound based on the elements in the solution on the surface of the iron-based matrix, which implies a rapid passivation of the material under test conditions in a saline solution, which confirms the observations made by microstructural analysis. Dendrite analyzes points 2 and 3, show oxidation of these metallic elements as well as the formation of stable chlorine-based compounds on the surface. It is also observed that in addition to the general oxidation of the chromium formations, there are zones, point 3, in which stable oxides are formed on the surface of the metallic material.

Figure 6 shows the distribution of the chemical elements identified on the cast iron surface C (Cr=21wt%) after corrosion.

In addition to the Fe-based matrix (fig. 6c) and Cr-based dendrites highlighted by the distributions in figure 6d, the oxides (fig. 6e) and chlorine-based compounds (fig. 6f) are observed. The intensity of the Cl and Cr signals shows that the thickness of the compound is greater than 5 μm, which will be analyzed later. It is noted that the oxidation is mainly performed on chromium dendrites.

Conclusions

From the analysis of the corrosion resistance of the experimental alloys we have highlighted the following:

- a selective attack in the saline solution was carried out; the surface of the iron-based matrix being intact from a microstructural point of view;

- It was observed that Cr-based dendrites were highlighted during the electro-corrosion test. The chemical composition obtained from the general surface area of the sample by the EDAX technique is close to the chemical composition obtained on the spark spectrometer and shows traces of new O, Na or Cl compounds;

- it was observed that on the surface of the iron-based matrix there are no traces of oxidation or compounds based on the elements in the solution, which implies a rapid passivation of the material under test conditions in a saline solution which confirms the observations made by the structural analysis;

- analyzes performed on dendritic compounds show oxidation of these metallic elements as well as formation of stable chlorine-based compounds on the surface. It has also been observed that in addition to the general oxidation of the chromium formations, there are also areas where stable oxides are formed on the surface of the metallic material.

References

1. DOGAN, O., HAWK, J., Wear, **189**, 1995, , pp.136–142.
2. SANDU, A.V., CIOMAGA, A., NEMTOI, C., BEJINARIU, C., SANDU, I., Journal of Optoelectronics and Advanced Materials, **14**, no. 7-8, 2012, pp. 704-708.
3. NEJNERU, C., VIZUREANU, P., SANDU, A.V., GRECU, A., CIMPOESU, N., Rev. Chim. (Bucharest), **65**, no. 2, 2014, pp. 194-198.
4 SANDU, A.V., CODDET, C., BEJINARIU, C., Journal of Optoelectronics and Advanced Materials, **14**, no. 7-8, 2012, pp. 699-703.
5. NICA, P.E., AGOP, M., GURLUI, S., BEJINARIU, C., FOCSA, C., Jpn. J. Appl. Phys., **51**, 2012, 106102.
6. CHEN, L., ZHOU, J., BUSHLYA, V., GUTNICHENKO, O., STAHL, Int. J. Adv. Manuf. Technol., **79**, 2015, pp. 635–644.
7. BUZEA, C.G., BEJINARIU, C., BORIS, C., VIZUREANU, P., AGOP, M., Int. J. Nonlinear Sci. Numer. Simul., **10**, 2009, pp. 1399–1414.
8. SUN, T., SONG, R., WANG, X., DENG, P., WU, C., J. Iron Steel Res. Int., **22**, 2015, pp. 84–90.
9. ATABAKI, M. M., JAFARI, S., ABDOLLAH-POUR, H., J. Iron Steel Res. Int., **19**, 2012, pp. 43–50.
10. LI, D., LIU, L., ZHANG, Y., YE, C., REN, X., YANG, Y., YANG, Q., Materials & Design **30**, no. 2, 2009, pp. 340–345.
11. OBERDORSTER, G., OBERDORSTER, E., OBERDORSTER, J., Environ. Health Perspect., **113**, 2005, pp. 823–839.
12. CIMPOESU, N., STANCIU, S., VIZUREANU, P., CIMPOESU, R., ACHITEI, D. C., IONITA, I., Obtaining Shape Memory Alloy Thin Layer Using Pld Technique, J. Min. Metall. Sect. B-Metall., **50**, 2014, pp. 69–76.
13. MONTGOMERY, D.C., Design and Analysis of Experiments, John Willey and Sons, 2004.
14. TANG, X. H., CHUNG, R., LI, D. Y., HINCKLEY, B., DOLMAN, K., Wear, **267**, 2009, pp. 116–121.
15. BURLEA, S. L., LEATA, R., AGOP, M., CIMPOESU, N., Rev. Chim. (Bucharest), **67**, no. 2, 2016, p. 260
16. BEJINARIU, C., SANDU, A.V., BACIU, C., SANDU, I., TOMA, S.L., SANDU, I.G., Rev. Chim. (Bucharest), **61**, 2010, p. 961
17. BACAITA, E.S., BEJINARIU, C., ZOLTAN, B., PEPTU, C., ANDREI, G., POPA, M., MAGOP, D., AGOP, M., J. Appl. Math., 2012, 653720.
18. CIMPOESU, N., TRINCA, L. C., DASCALU, G., STANCIU, S., GURLUI, S. O., MARECI, D., Journal of Chemistry, 2016, 9520972.
19. MARECI, D., CIMPOESU, N., POPA, M. I., Materials Corrosion, **63**, 2012, pp. 985–991.
20. ACHITEI, D.C., VIZUREANU, P., DANA, D., CIMPOESU, N., Metalurgia International, **18**, SI2, 2013, p. 104.
21. ACHITEI, D.C., VIZUREANU, P., MINCIUNA, M.G., SANDU, A.V., BUZAIANU, A., DANA, D.I., Materiale Plastice, **52**, no. 2, 2015, p. 165.
22. ACHITEI, D.C., VIZUREANU, P. STANCIU, S., STEFANICA, R.G., CIMPOESU, N., Modtech 2010: New Face of TMCR, Proceedings of the International Conference ModTech, 2010, p. 15.
23. SANDU A.V., CODDET C., BEJINARIU C., Rev. Chim. (Bucharest), **63**, no. 4, 2012, p. 401
24. SANDU, A.V., CIOMAGA, A., NEMTOI, G., BEJINARIU, C., SANDU, I., Microscopy Research And Technique, **75**, no. 12, 2012, p. 1711-1716
25. RAMBU, A.P., SIRBU, D., SANDU, A.V., PRODAN, G., NICA, V., Bulletin of Materials Science, **36**, no. 2, 2013, p. 231.
26. VIZUREANU, P., Metalurgia International, **14**, no. 5, 2009, p. 5.

Manuscript received: 15.03.2017